# Cluster size regulates protein sorting in the immunological synapse

Niña C. Hartman[a], Jeffrey A. Nye[b], and Jay T. Groves[a,c,d,1]

Departments of [a]Chemistry and [b]Chemical Engineering, [c]Howard Hughes Medical Institute, and [d]Physical Biosciences and Materials Sciences Divisions, Lawrence Berkeley National Laboratory, University of California, Berkeley, CA 94720

Edited by Douglas T. Fearon, University of Cambridge, Cambridge, United Kingdom, and approved June 18, 2009 (received for review March 12, 2009)

**During antigen recognition by T cells, signaling molecules on the T cell engage ligands on the antigen-presenting cell and organize into spatially distinctive patterns. These are collectively known as the immunological synapse (IS). Causal relationships between large-scale spatial organization and signal transduction have previously been established. Although it is known that receptor transport during IS formation is driven by actin polymerization, the mechanisms by which different proteins become spatially sorted remain unclear. These sorting processes contribute a facet of signal regulation; thus their elucidation is important for ultimately understanding signal transduction through the T cell receptor. Here we investigate protein cluster size as a sorting mechanism using the hybrid live T cell–supported membrane system. The clustering state of the co-stimulatory molecule lymphocyte function-associated antigen-1 (LFA-1) is modulated, either by direct antibody crosslinking or by crosslinking its intercellular adhesion molecule-1 ligand on the supported bilayer. In a mature IS, native LFA-1 generally localizes into a peripheral ring surrounding a central T cell receptor cluster. Higher degrees of LFA-1 clustering, induced by either method, result in progressively more central localization, with the most clustered species fully relocated to the central zone. These results demonstrate that cluster size directly influences protein spatial positioning in the T cell IS. We discuss a sorting mechanism, based on frictional coupling to the actin cytoskeleton, that is consistent with these observations and is, in principle, extendable to all cell surface proteins in the synapse.**

actin | mechanobiology | membrane | transport | receptor

Despite their dynamic liquid nature, cell membranes exhibit distinctive spatial organization on length scales ranging from molecular dimensions to the size of the cell itself. One particularly dramatic example is the T cell immunological synapse (IS). This structure is a specialized junction between a T cell and an antigen-presenting cell (APC), within which a variety of receptor and adhesion proteins engage their cognate ligands on the apposed cell surface (1, 2). Before contact, no large-scale organization is present on either cell surface. However, within minutes of the initial encounter between an APC displaying appropriate antigen and a complementary T cell, a highly coordinated transport process is initiated that ultimately sorts dozens of membrane proteins on both cell surfaces into a series of concentric rings. This spatial pattern of proteins is not unique to T cells; similar structures have also been observed between natural killer cells and B cells and their target cells, as well as between certain immune cells and neurons (3, 4). Recent work has demonstrated the importance of protein spatial distribution to both effector functions and as a signal regulatory mechanism (5–7). However, the mechanism of IS formation is unclear.

In the case of the T cell-B cell interaction, the rapid spatial sorting of cell membrane proteins into multiple specific regions within the intercellular junction is driven from within the T cell (8). Substitution of the B cell with a synthetic supported lipid bilayer (SLB) displaying key proteins produces minimal differences in the antigen specificity or protein spatial organization (2). The transport mechanism is postulated to be based on actin polymerization and the resulting centripetal actin flow within the T cell (8–10). Disruption of this actin flow using cytoskeletal inhibitors blocks transport (8, 10). Associations of cell-surface proteins with actin are thought to exist via adaptor proteins, such as talin, which is known to couple lymphocyte function-associated antigen-1 (LFA-1) to the actin cytoskeleton (11). Similarly, ezrin has been reported to be an adaptor protein for the T cell receptor (TCR) (12). Although simply coupling to actin flow may be sufficient for protein transport, additional regulation is required to achieve differential sorting of multiple proteins within the IS.

Differential protein sorting is markedly illustrated by comparison of TCR and LFA-1, which become segregated into the central supramolecular activation cluster (cSMAC) and the surrounding peripheral supramolecular activation cluster (pSMAC), respectively (1, 2). Direct tracking of TCR and LFA-1 motion on the cell surface reveals that these 2 proteins move in the same direction under the influence of centripetal F-actin flow (9, 10, 13). The mechanism directing them to different destinations, microns apart, remains mysterious. Before transport, TCR engagement of the peptide-major histocompatibility complex (pMHC) on the apposed membrane leads to the formation of TCR clusters that contain approximately 100 TCR molecules, which are subsequently transported to the cSMAC (9, 14). LFA-1 does not form such large-scale clusters upon binding its ligand, intercellular adhesion molecule-1 (ICAM-1) (11, 15). Thus, we speculate that differences in cluster size may contribute to protein sorting.

In the present study, we manipulate the clustered state of LFA-1 in primary murine T cells to directly investigate the effect of protein cluster size on spatial sorting. Cluster size is increased by crosslinking LFA-1 with a non-blocking bivalent monoclonal antibody (Bi-X LFA-1). Crosslinking the primary antibody with a secondary antibody to form a tetravalent crosslinker against LFA-1 leads to a more clustered state (Tetra-X LFA-1). Thus, 2 degrees of clustering beyond the native state, which may already be clustered to a small degree, are accessible. Compared with non-crosslinked LFA-1, Bi-X LFA-1 is transported further inward toward the inner zone of the pSMAC, immediately surrounding the cSMAC. Crosslinking with a tetravalent agent leads to localization of LFA-1 to the cSMAC along with TCR. Use of bivalent and tetravalent crosslinkers against ICAM-1 induces similar alterations in the spatial position of LFA-1:ICAM-1 complexes. Thus, increasing the clustering state of LFA-1, either directly by using anti-LFA-1 antibodies or indirectly by crosslinking its ICAM-1 ligand, biases its distribution toward the synapse center. Moreover, spatial sorting of the

Author contributions: N.C.H., J.A.N., and J.T.G. designed research; N.C.H. and J.A.N. performed research; N.C.H., J.A.N., and J.T.G. analyzed data; and N.C.H., J.A.N., and J.T.G. wrote the paper.

The authors declare no conflict of interest.

This article is a PNAS Direct Submission.

[1]To whom correspondence should be addressed. E-mail: jtgroves@lbl.gov.

This article contains supporting information online at www.pnas.org/cgi/content/full/0902621106/DCSupplemental.

differentially crosslinked LFA-1 species from each other within a single synapse is also observed. These results illustrate that differences in protein cluster size are sufficient to direct discrete sorting of proteins into different regions of the IS. We discuss how a frictional mechanism for coupling of proteins to centripetal actin flow, which may apply generally to many proteins in the synapse, predicts this.

## Results

**ICAM-1 Distribution Reflects Ligated LFA-1 Pattern on the T Cell.** The formation of LFA-1:ICAM-1 complexes is necessary for the recruitment of active LFA-1 and ligated ICAM-1 to the pSMAC (7). During cell migration and upon TCR activation, LFA-1 binds ICAM-1 and induces its accumulation on the apposed surface in contact with the T cell membrane (11). This interaction depletes the local concentration of unbound ICAM-1 molecules, which further drives the diffusive flux of free ICAM-1 into the contact area by the law of mass action (16). The total ICAM-1 distribution thus reflects the pattern of active, ligated LFA-1 on the T cell surface. To confirm that the ICAM-1 pattern provides a real-time means of tracking ligated LFA-1 on the T cell, we monitor its reversibility of binding to crawling T cells. We use an ICAM-1-YFP fusion protein linked to nickel-chelating lipids in the SLB by a stable decahistidine tag (17). Although the commonly used H155 antibody for LFA-1 also allows for direct tracking, it indiscriminately binds both active (ICAM-1 bound) and inactive (non-ICAM-1 bound) forms of LFA-1 (18). To quantitatively characterize ICAM-1 fluorescence as a function of its interactions with LFA-1 on T cells, we deposit the SLB on substrates pre-patterned with grid arrays of metal lines (3 $\mu$m $\times$ 3 $\mu$m corrals) that act as barriers to lateral mobility. Membrane lipids and proteins diffuse normally within each corral (6, 19). A constant number of freely mobile ICAM-1 molecules are thus trapped within each corral (Fig. 1 and Fig. S1) (20–22). Restriction of ICAM-1 and pMHC lateral motion within the SLB by the metal grid lines indirectly disrupts the transport of bound cognate receptors on the T cell (Fig. 1*A*). Receptor-ligand pairs do not directly interact with the metal lines and are affected solely by restriction of their lateral mobility (6, 19).

Initially, ICAM-1 accumulates beneath the crawling T cell and the area of ICAM-1 accumulation decreases in size as the cell migrates away from the corral. Without T cell contact (t = 110 sec; Fig. 1*C*), ICAM-1 rapidly returns to a homogeneous distribution by passive diffusion. The total integrated fluorescence, relative to off-grid ICAM-1, remains constant, confirming that fluorescence intensity linearly maps ICAM-1 concentration. No measurable quenching is observed, nor does ICAM-1 desorb from the membrane over the course of these experiments (see Fig. S1 for ensemble data from a population of cells). These results confirm that ICAM-1 spatial distribution quantitatively reflects the distribution of LFA-1:ICAM-1 complexes.

**LFA-1 Is Transported Inward During IS Formation.** In the native IS, LFA-1:ICAM-1 complexes form a ring at the pSMAC and TCR:pMHC micro-clusters congregate into a central cluster at the cSMAC (Fig. 2*A*). Synapse assembly on substrates displaying diffusion barriers leads to altered protein patterns in the final IS, which we refer to as spatial mutations (6). Specific features of the spatial mutation reveal aspects of the mechanism that drives synapse assembly. Here, the inward radial transport of both TCR:pMHC and LFA-1:ICAM-1 complexes is made apparent by TCR and ICAM-1 accumulation in areas along the grid lines that are closest to the synaptic center (Fig. 2*B*). Similar evidence of LFA-1 inward transport is observed by directly labeling LFA-1 with H155 antibody (Fig. S2). These observations confirm that both LFA-1 and TCR are transported in an inward radial manner during synapse formation in primary T cells by processes that

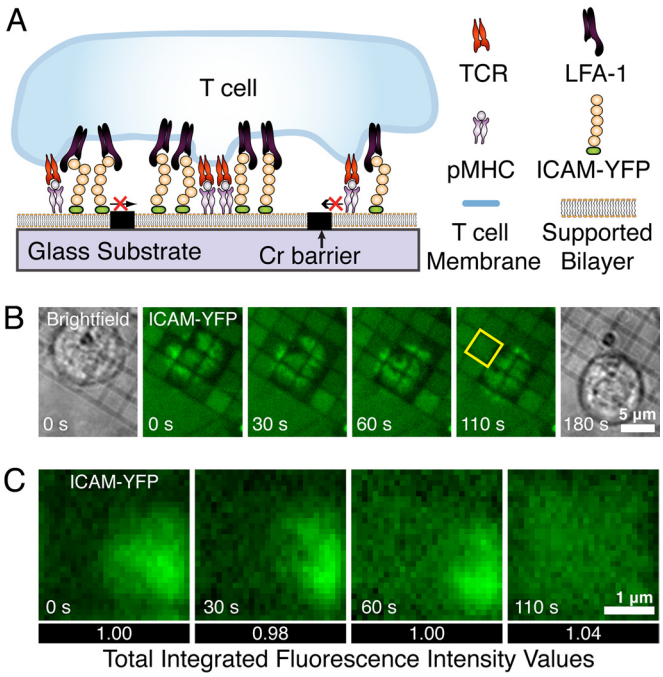


**Fig. 1.** ICAM-1 distribution reflects the ligated LFA-1 pattern on the T cell. (*A*) Diagram of a T cell exposed to a planar bilayer on a patterned substrate. Proteins on the T cell engage their cognate ligands and are constrained by the diffusion barriers. (*B*) A cell migrates over a supported bilayer containing ICAM-1 and pMHC corralled by metal lines into 3 $\mu$m squares. As the cell moves, ICAM-1 distribution within the corrals changes as a result of LFA-1 binding. When the cell is no longer in contact with the grid square, ICAM-1 is released and diffuses back to homogeneity. (*C*) Magnified images of the 3-$\mu$m $\times$ 3-$\mu$m square indicated in *B*. Total integrated fluorescence within the corral indicated, normalized to t = 0, is given beneath each image, showing that clustering does not significantly affect total ICAM-1 fluorescence.

resemble those previously reported from tracking experiments in Jurkat cells (10). Disruption of pattern formation by addition of the actin polymerization blocker latrunculin A confirms that inward transport is mediated by actin centripetal flow (Fig. S3).

**TCR-pMHC Micro-Clusters Exclude and Displace LFA-1:ICAM-1 Complexes.** Simultaneous imaging of TCR and ICAM-1 reveals exclusion of LFA-1:ICAM-1 complexes by TCR micro-clusters.

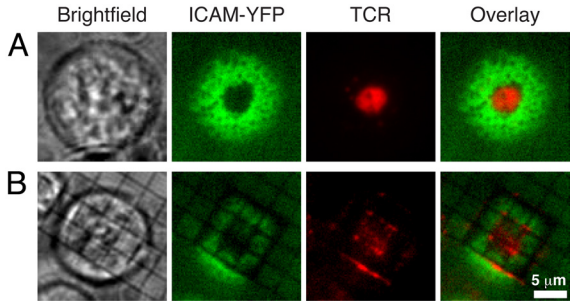


**Fig. 2.** LFA-1 is transported inward during IS formation. (*A*) In an unperturbed IS, LFA-1:ICAM-1 complexes form a ring, as visualized with ICAM-YFP, and TCR labeled with H57 $\alpha$TCR-$f_{ab}$ (Alexa Fluor 568) forms a central cluster (observed in 75% of T cells, $n$ = 81). (*B*) Upon T cell interaction with an SLB constrained by metal grid lines, LFA-1:ICAM-1 complexes and TCR accumulate in areas closest to the synaptic center (observed in 80% of T cells, $n$ = 41). Throughout the interface, TCR displaces LFA-1:ICAM-1 complexes to occupy the most central position available. Images were taken using epifluorescence microscopy.

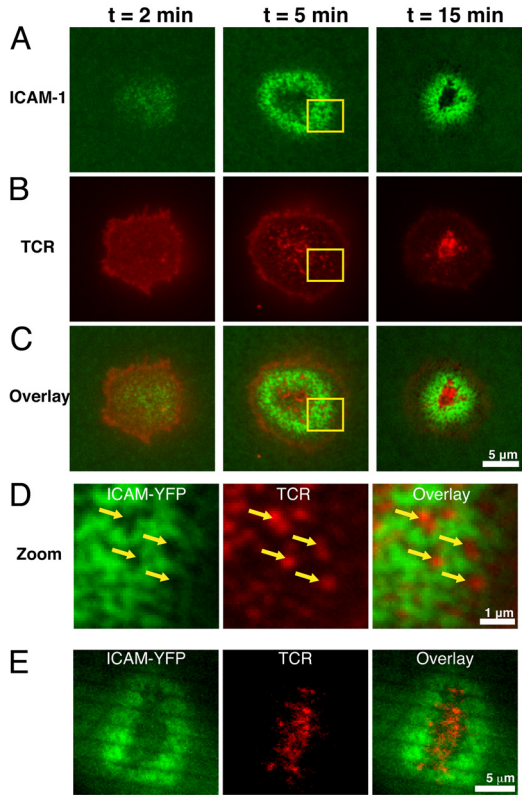


**Fig. 3.** TCR micro-clusters exclude and displace LFA-1:ICAM-1 complexes. Epifluorescence images of ICAM-YFP (*A*) and T cells labeled with labeled $\alpha$TCR-$f_{ab}$ (Alexa Fluor 568) (*B*) that were fixed 2 min (column 1), 5 min (column 2), and 15 min (column 3) after contact with SLBs containing ICAM-1 and pMHC. Upon formation, TCR micro-clusters exclude and displace ICAM-1 as they translocate to the cSMAC. The ICAM-1 density within the excluded areas is comparable to the bulk density. (*C*) Composite image of ICAM-1 from *A* and TCR from *B*. (*D*) Magnified images of the area indicated in *C* of the T cell fixed after 5 min. (*E*) Fluorescent images taken with TIRF illumination of ICAM-YFP and TCR on live T cells exposed to a bilayer constrained by diffusion barriers (parallel lines with 2 $\mu$m spacing). Within the pSMAC, TCR:pMHC micro-clusters occupy the most central positions and exclude LFA-1:ICAM-1 complexes.

Upon initial cell contact with the bilayer, ICAM-1 begins to accumulate and TCR assembles into micro-clusters at the interface (Fig. 3 *A–C*, column 1; observed in 90% of cells, $n = 44$). After 5 min of cell interaction with the bilayer, 67% of the cells ($n = 122$) contain voids (<300 nm in diameter) within the ICAM-1 ring that colocalize with the TCR:pMHC micro-clusters (Fig. 3 *A–C*, column 2; and magnified images in Fig. 3*D*). The ICAM-1 density within these voids is comparable to bulk density, indicating that unligated ICAM-1 is free to diffuse throughout the interface while LFA-1:ICAM-1 complexes are specifically excluded. Nascent TCR:pMHC micro-clusters continue to colocalize with the voids in the LFA-1:ICAM-1 ring after 15 min (Fig. 3 *A–C*, column 3) of cell interaction with the SLB (observed in 77% of cells, $n = 196$).

LFA-1 and TCR do not translocate together, although both are transported inward in an actin-dependent manner. Moreover, the larger TCR:pMHC micro-clusters efficiently displace LFA-1:ICAM-1 complexes within the relatively static pSMAC (Movie S1 and Fig. S4). In addition to this dynamic displacement, we observe a static exclusion and spatial sorting between these proteins within peripheral regions of the synapse when substrate barriers block further inward transport (Fig. 3*E*). Note how TCR:pMHC micro-clusters out-compete LFA-1:ICAM-1 complexes for the innermost positions within each corralled zone (observed in 66% of cells, $n = 101$). We also show a similar observation for differentially clustered, ligated LFA-1 (Fig. 5*G*). An important corollary of this observation is that segregation between the pSMAC and cSMAC is not driven exclusively by an internal difference in cellular structure between these 2 regions. From these observations, we conclude that an active differential sorting mechanism capable of distinguishing between TCR:pMHC micro-clusters and LFA-1:ICAM-1 complexes exists throughout the synaptic interface.

**Cluster Size Determines LFA-1 Spatial Sorting in the IS.** We manipulated the cluster size of LFA-1 to determine its effect on LFA-1 transport and radial distribution. LFA-1 distribution at the pSMAC is typically observed using the non-crosslinking H155 $f_{ab}$ fragments ($\alpha$LFA-$f_{ab}$), which are monovalent and lack the $f_c$ portion (Fig. S5*A*) (5, 18). Crosslinking LFA-1 with the H155 bivalent antibody ($\alpha$LFA-mAb) increases its cluster size (Bi-X LFA-1). The $\alpha$LFA-mAb may be crosslinked itself by a secondary antibody ($\alpha$mAb), which specifically binds to the $f_c$ portion. T cell incubation with this tetravalent crosslinker further increases the degree of LFA-1 clustering (Tetra-X LFA-1).

Cluster size-based protein sorting is observed by simultaneously labeling LFA-1 with $f_{ab}$ fragments (No-X LFA-1) and either the bivalent or tetravalent crosslinker. Before interaction with the SLB, live T cells were concurrently incubated with fluorescently labeled H155 $\alpha$LFA-mAb and $\alpha$LFA-$f_{ab}$. No-X LFA-1 displayed the native broad annular pattern at the pSMAC. Bi-X LFA-1 also sorted into the pSMAC. However, the Bi-X LFA-1 clusters were transported further inward, leading to an enriched ring pattern in the inner zone of the pSMAC (Fig. 4*B*). Tetra-X LFA-1 localized in the cSMAC, where TCR:pMHC micro-clusters are recruited (Fig. 4*C*). Labeling with the different crosslinkers in the absence of LFA-1 pre-clustering did not result in the observed differences in LFA-1 spatial patterns (Fig. S6). The differential sorting can be quantified for a population of cells by generating averaged protein density plots of the normalized and azimuthally integrated intensities obtained for the various forms of LFA-1 as a function of the normalized cell radii (Fig. 4*D Inset*). These averaged radial profiles ($n = 53$ cells each) of the Bi-X LFA-1 (Fig. 4*D*) and Tetra-X LFA-1 (Fig. 4*E*), compared with the radial profile of No-X LFA-1, reveal the different characteristic spatial sorting as a function of cluster size. The mean normalized radii at which peak intensities (i.e., maximum protein concentrations) occur for each case ($\pm$SE) are clearly different with the more inward positions occupied by the more highly crosslinked species ($P < 0.001$ for both sets, Student *t* test). Slight differences between the mean radial positions at peak intensities for the No-X LFA-1 may occur as a result of No-X LFA-1 exclusion from the inner pSMAC zone by the Bi-X LFA-1.

The overall synapse morphologies of ICAM-1 (pSMAC) and TCR (cSMAC) are largely unaffected by the induced clustering of a subpopulation of LFA-1 in these experiments (Fig. 4*F*). The unaltered distribution of ICAM-1 at the pSMAC for all degrees of crosslinking applied (Fig. S5 *B* and *C*) indicates that a sufficient population of non-crosslinked and unlabeled ligated LFA-1 is present to preserve the broad pSMAC pattern. Direct crosslinking of LFA-1 may preferentially sort unligated LFA-1 to the cSMAC given that ICAM-1 accumulation, which maps only ligated LFA-1, does not reflect the distributions of crosslinked LFA-1 at the IS.

**Crosslinked ICAM-1 Increases Inward Transport of Active LFA-1.** To selectively study crosslinking effects on LFA-1 ligated to ICAM-1, we used a bivalent crosslinking antibody against the YFP domain ($\alpha$YFP-mAb) of the ICAM-1-YFP fusion protein. Crosslinked ICAM-1 (Bi-X ICAM-1) is formed by incubation of the bilayer containing ICAM-YFP and pMHC with $\alpha$YFP-mAb

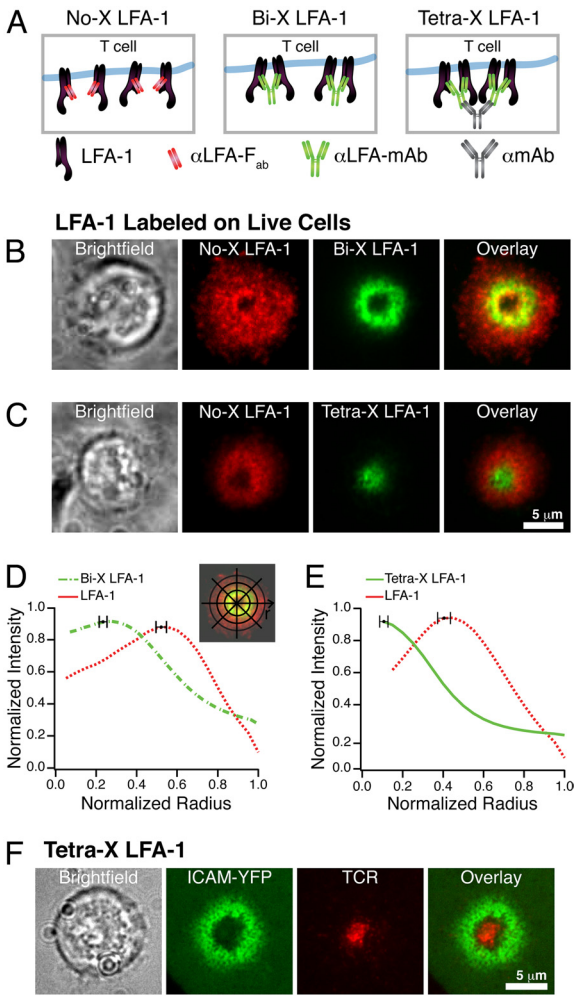


**Fig. 4.** Increased clustering of LFA-1 changes its spatial localization. LFA-1 was labeled in live cells (*B* and *C*) and imaged with TIRF microscopy. (*A*) Diagram of the degrees of LFA-1 clustering. (*B*) T cells were labeled with H155 αLFA-f$_{ab}$ fragment (No-X LFA-1) and αLFA-mAb (Bi-X LFA-1). (*C*) H155 αLFA-mAb was pre-clustered by crosslinking with an antibody (αmAb) and T cells were labeled as in *B* to give No-X LFA-1 and Tetra-X LFA-1. Averaged radial profile plots ($n = 53$ cells each) of intensities as a function of the normalized cell radii obtained for Bi-X LFA-1 (*D*) and Tetra-X LFA-1 (*E*) compared with No-X LFA-1. (*Inset*) The integrated intensity is the sum of the pixel values along each circle at a given radius and is normalized by the number of pixels in the circle. The mean peak intensities (±SE) are shown ($P < 0.001$, Student *t* test). Data are representative of 3 independent experiments. (*F*) For T cells incubated with the tetravalent crosslinker, the ICAM-1 ring and TCR central cluster is maintained. Thus, ICAM-1 and TCR synapse morphology is unaffected by crosslinking a subpopulation of cell-surface LFA-1.

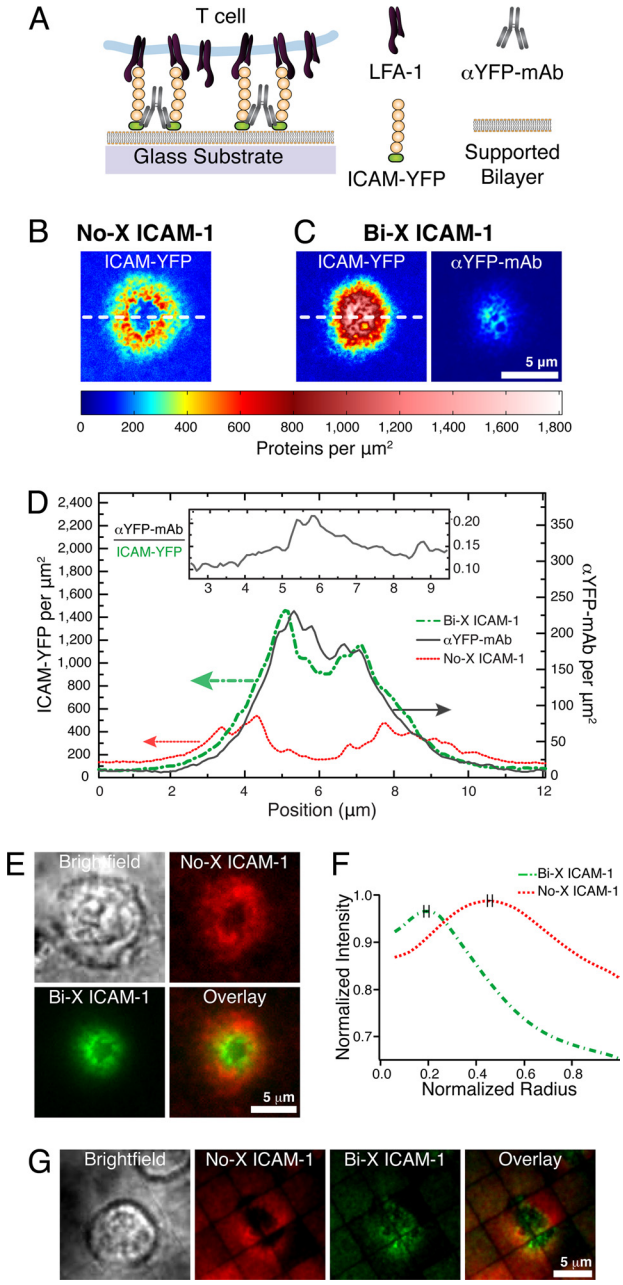


**Fig. 5.** Crosslinking ICAM-1 alters synapse morphology. (*A*) Diagram of ICAM-YFP crosslinked with αYFP-mAb (Bi-X ICAM-1). (*B*) Quantitative protein density map of ICAM-YFP in a native synapse and (*C*) ICAM-YFP and αYFP-mAb (Alexa Fluor 568) in a synapse with Bi-X ICAM-1. Images were taken by epifluorescence microscopy. (*D*) Line scans through the center of each cell plot ICAM-YFP density (left axis) and αYFP-mAb density (right axis). (*Inset*) Plot of αYFP-mAb/ICAM-YFP using line scan values for areas within the cell. (*E*) Bi-X ICAM-1 and non-crosslinked ICAM-1 (No-X ICAM-1) are simultaneously presented on the bilayer before T cell addition. (*F*) Average radial profiles of No-X ICAM-1 and Bi-X ICAM-1 with mean peak integrated intensity (±SE) are shown and were obtained as in Fig. 4 ($P < 0.001$, Student *t* test). Data are representative of 5 independent experiments. (*G*) Bi-X ICAM-1 and No-X ICAM-1 sorting are also shown for when the bilayer is corralled by 5-$\mu$m × 5-$\mu$m grid squares. As seen with TCR and ICAM-1, Bi-X ICAM-1 occupies the most radially inward positions along the grid lines within the pSMAC, displacing No-X ICAM-1.

before T cell addition (Fig. 5*A*). The different spatial distributions of LFA-1:ICAM-1 complexes, as a function of ICAM-1 crosslinking, are evident in the quantitative fluorescence images presented in Fig. 5. These images are calibrated to reveal absolute protein densities using a method based on supported bilayer standards (23). Imaging the fluorescently labeled αYFP-mAb responsible for crosslinking the ICAM-YFP reveals that it is primarily concentrated in the cSMAC (Fig. 5*C Right*). Line scans of protein densities along the dashed lines on Fig. 5 *B* and *C* are also shown in Fig. 5*D*. An ICAM-1:αYFP-mAb ratio greater than 2:1 requires that additional ICAM-1 be indirectly linked through LFA-1 linkages in the T cell. The approximate 6:1 ICAM-YFP:αYFP-mAb ratio observed in the cSMAC (Fig. 5*D Inset*) provides evidence for native LFA-1 organization into preexisting clusters of no more than a few molecules (11, 15). These observations indicate that LFA-1:ICAM-1 complexes, which have been crosslinked through ICAM-1, preferentially

segregate closer to the cSMAC, whereas non-crosslinked LFA-1:ICAM-1 complexes primarily populate the pSMAC. The use of a tetravalent crosslinker against ICAM-1 (Tetra-X ICAM-1) results in complete transport of ICAM-1 to the cSMAC (Fig. S7). Cytosolic calcium levels, used to measure cell signaling, do not differ between cells interacting with Tetra-X ICAM-1 and cells forming native patterns (Fig. S8). Addition of latrunculin A to T cells interacting with these differently crosslinked ICAM-1 species result in synaptic patterns that are not well resolved (Fig. S3 *B* and *C*).

Protein sorting between crosslinked and non-crosslinked ICAM-1 can be directly observed when both populations simultaneously interact with a T cell. Bilayers containing pMHC, fluorescently labeled ICAM-1 (Alexa Fluor 647) lacking the YFP moiety (No-X ICAM-1), and ICAM-YFP (Bi-X ICAM-1) are incubated with $\alpha$YFP-mAb before T cell addition. Upon T cell activation, the Bi-X ICAM-1 can be seen to segregate from the No-X ICAM-1 (Fig. 5*G*). The more centrally biased distribution of LFA-1:Bi-X ICAM-1 relative to the LFA-1:No-X ICAM-1 is also evident in the cell population-averaged radial profiles (Fig. 5*F*, $n = 63$, mean $\pm$ SE). No-X ICAM-1 fluorescence intensities in the cSMAC are comparable to bulk intensity values, indicating free diffusion of unligated ICAM-1 throughout the synaptic junction. When the same bilayer system is constrained into patterned grid arrays of diffusion barriers, LFA-1:Bi-X ICAM-1 complexes clearly occupy the most radially inward positions along the barriers and exclude LFA-1:No-X ICAM-1 complexes (Fig. 5*H*). Crosslinking alters the clustering state of ligated LFA-1, and the cell transports crosslinked LFA-1:ICAM-1 complexes further inward than non-crosslinked ICAM-1.

## Discussion

Upon T cell activation, LFA-1 and TCR engage their ligands and become sorted into the pSMAC and cSMAC by radial transport within the T cell-APC junction. Direct or indirect external crosslinking of LFA-1 on T cells preceding IS formation alters its spatial sorting. Specifically, we have observed a graduated response in which a bivalent crosslinker redirects LFA-1:ICAM-1 complexes to the innermost radii of the pSMAC whereas a tetravalent crosslinker causes them to localize in the cSMAC. These results indicate that the crosslinking state of LFA-1 can determine its final position within the IS.

We propose a mechanistic model whereby the sorting of proteins results from differential strengths of coupling to the moving actin cytoskeletal network. Linking of cell surface proteins to actin (e.g., via talin, ezrin, or other less direct methods) may be described as frictional coupling (24, 25). The result is that a protein, or cluster of proteins, on the cell surface experiences a driving force in the direction of actin cytoskeletal flow. If individual bonds form and break rapidly, it is not necessary that the proteins be driven at the same speed, or even in the same direction, as the actin flow. Indeed, it has been previously reported that TCR clusters can be driven at angles to the preferred flow when they encounter physical barriers (13). If we speculate that the strength of coupling to the cytoskeleton exhibits a nonlinear scaling with protein density (e.g., there is a degree of cooperative binding), the result is a cluster size-mediated sorting of the type observed in the experiments described here.

Under such a mechanism, all proteins in the membrane will experience a driving force determined by the composite of their specific coupling chemistry to the actin network and their local clustering state. The transport progresses until a quasi-equilibrium radial distribution is reached in which the inward driving force of each protein cluster species is balanced by local competition from surrounding clusters. This is analogous to sedimentation equilibrium, in which denser species out-compete less dense species for the down-field positions in a force field (e.g., centrifugal, gravitational, electric) (26, 27). In the case of the T cell IS, the driving force is the actin cytoskeletal flow and the coupling force per unit area experienced by the protein clusters determines their relative positions. TCR clusters clearly have a higher coupling force density than native LFA-1:ICAM-1 complexes. This conclusion is partly based on our observations of the ability of TCR clusters to physically displace LFA-1:ICAM-1 en route to the cSMAC (Movie S1 and Fig. S4). Additionally, TCR trapped in the pSMAC region on patterned substrates displace LFA-1 from the innermost radial positions of each corral (see Fig. 2*B* and Fig. 3*E*). For the same reasons, TCR clusters, along with other cSMAC localizing proteins, such as CD28:B7–1 (28) (Fig. S9), could prevent the more weakly coupled LFA-1 from entering the cSMAC (Fig. 6*A*). External crosslinking of LFA-1 into larger clusters increases the coupling force density, enabling LFA-1 clusters to effectively compete with TCR for cSMAC territory (Fig. 6 *B* and *C*). The mechanism we suggest here is consistent with all the observations discussed. However, other mechanisms have also been proposed.

Size exclusion and membrane bending effects have long been considered as possible contributors to protein sorting within the IS (29–32). It has been suggested that the larger ectodomains of LFA-1:ICAM-1 complexes ($\approx$42 nm) prevent their colocalization with TCR:pMHC complexes ($\approx$15 nm) at the cSMAC.

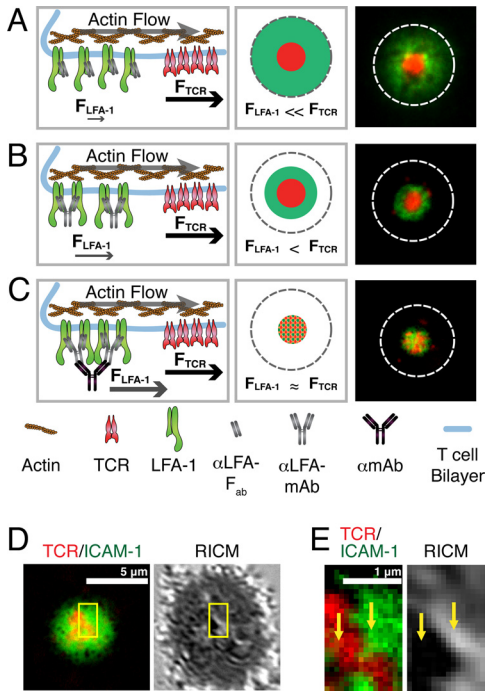


**Fig. 6.** Schematic of the model for protein sorting in IS formation. LFA-1 and TCR transport are coupled to actin centripetal flow and the strength of actin attachment scales with the protein cluster size. (*A*) Micro-clusters of TCR and relatively non-clustered LFA-1 molecules are transported inward and TCR forms a central cluster in the cSMAC surrounded by a ring of LFA-1 in the pSMAC. (*B*) Crosslinking of LFA-1 with a bivalent crosslinker increases its coupling to actin, resulting in LFA-1 accumulation in the inner zone of the pSMAC. (*C*) Crosslinking LFA-1 with a tetravalent crosslinker forms large LFA-1 clusters, leading to comparable coupling strengths of LFA-1 and TCR to actin. Both TCR and LFA-1 occupy the cSMAC. (*D*) Fluorescence images of the small-scale segregation between TCR:pMHC (red) and LFA-1:ICAM-1 (green) complexes in the cSMAC. The RICM image reveals membrane topography and darker areas indicate closer membrane interactions. (*E*) Magnified fluorescence and RICM images of the area indicated in *D*. TCR:pMHC complexes colocalize with darker regions in the RICM and LFA-1:ICAM-1 complexes colocalize with the lighter regions.

Observation of LFA-1:Tetra-X ICAM-1 clusters in the cSMAC suggests that size exclusion alone is insufficient to define cSMAC composition. Additionally, topographic imaging of this altered cSMAC region by reflection interference contrast microscopy (RICM) indicates that membrane topography conforms to the interleaved protein composition (Fig. 6 *D* and *E*). Although size exclusion may be a factor in protein segregation over shorter length scales, it is not the primary force behind cSMAC formation. A more recently proposed hypothesis suggests that cluster stability may contribute a differentiating characteristic that targets LFA-1 and TCR to the pSMAC and cSMAC, respectively (10). In this model, sorting occurs because LFA-1 clusters need actin for stability but TCR clusters do not, allowing TCR to enter the actin-deficient cSMAC while LFA-1 cannot. Our observation of externally crosslinked LFA-1 entering the cSMAC is consistent with this hypothesis. However, the additional stratification and exclusion we observe of non-crosslinked, active LFA-1 by the species coupled to a bivalent crosslinker within the pSMAC is more difficult to account for based on cluster stability alone (Fig. 5*H*). We thus conclude that, although cluster stability will certainly contribute to spatial sorting, differential stability is not required for sorting. The predominant discrimination mechanism operating over most of the synaptic junction appears to be based on overall strength of protein coupling to actin. A compelling feature of the relatively simple frictional coupling mechanism is the ease with which it could be used by all proteins within the IS.

## Methods

Primary T cells directly harvested from splenocytes of first-generation AND × B10.BR transgenic mice were expanded to T cell blasts and maintained as described (6, 19). This protocol is approved by the Animal Welfare and Research Committee under Protocol 17702. Coverslips patterned with metal lines were made as before (6, 13) and used as the bottom face of a temperature-controlled flow cell chamber. Substrates were etched in piranha solution (3:1 $H_2SO_4$:$H_2O_2$), rinsed with $H_2O$, and dried under a stream of $N_2$ gas. Histidine-tagged ICAM-1, ICAM-1-YFP fusion protein, and MHC Class II I-$E^K$ were expressed and purified as before (17). Full-length and $f_{ab}$ fragments of H155 anti-LFA-1 and H57 anti-TCR antibodies were prepared by standard protocols. Moth cytochrome *c* (MCC) 88–103 peptide was loaded into the MHC by overnight incubation at 100 $\mu$M at 37 °C in pH 4.5 citrate buffer. DOPC (1,2-dioleoyl-sn-glycero-3-phosphocholine) bilayers comprised of 2 mol% $Ni^{2+}$-NTA-DOGS were prepared by standard methods. SLBs were incubated with ICAM-1 and MHC for 1 h in Tris buffer. The flow cell was heated to 37 °C and rinsed with 10 mL buffer before the addition of T cells. For crosslinking experiments, T cells or ICAM-1 on the SLB were incubated for 20 min with the crosslinking agents before cell interaction with the bilayer, as indicated. Tetravalent crosslinkers were formed by incubating the primary antibodies with the secondary antibodies for 20 min before incubation with the cells or the SLB. Total internal reflection fluorescence microscopy (TIRF) images were acquired on a Nikon TE2000 inverted microscope with a 100 × 1.49 NA oil immersion TIRF objective and a Cascade 512B EMCCD camera (Roper). Epifluorescence images were taken on Nikon TE300 inverted microscope with a 100 × 1.3 NA oil immersion objective and a CoolSnapHQ Camera (Photometrics). Data were acquired with the MetaMorph software package (Molecular Devices). Radial profile analysis was performed using the radial profile plug-in for ImageJ software (33). A more detailed *Materials and Methods* section is part of the *SI Text*.

**ACKNOWLEDGMENTS.** This work was supported by the Chemical Sciences, Geosciences and Biosciences Division, Office of Basic Energy Sciences, of the U.S. Department of Energy under Contract No. DE-AC03–76SF00098. Patterned substrates were made by B.L. Jackson and R. Petit in the University of California, Berkeley, Microlab and Lawrence Berkeley National Laboratory Molecular Foundry. The authors thank M.B. Forstner, M. Davis, B. Lillemeier, Boryana Manz, J.P. Hickey, A. Smoligovets, E. Liu, L. Mahadevan, R. Varma, T. Starr, and M.L. Dustin for helpful discussions, reagents, and technical help.

1. Monks CRF, Freiberg BA, Kupfer H, Sciaky N, Kupfer A (1998) Three-dimensional segregation of supramolecular activation clusters in T cells. *Nature* 395:82–86.
2. Grakoui A, et al. (1999) The immunological synapse: a molecular machine controlling T cell activation. *Science* 285:221–227.
3. Davis DM (2002) Assembly of the immunological synapse for T cells and NK cells. *Trends Immunol* 23:356–363.
4. Batista FD, Iber D, Nereberger MS (2001) B cells acquire antigen from target cells after synapse formation. *Nature* 411:489–494.
5. Lee KH, et al. (2003) The immunological synapse balances T cell receptor signaling and degradation. *Science* 302:1218–1222.
6. Mossman KD, Campi G, Groves JT, Dustin ML (2005) Altered TCR signaling from geometrically repatterned immunological synapses. *Science* 310:1191–1193.
7. Graf B, Bushnell T, Miller J (2007) LFA-1 mediated T cell costimulation through increased localization of TCR/class II complexes to the cSMAC and exclusion of CD45 from the immunological synapse. *J Immunol* 179:1616–1624.
8. Billadeau DD, Nolz JC, Gomez TS (2007) Regulation of T-cell activation by the cytoskeleton. *Nat Rev Immunol* 7:131–143.
9. Varma R, Campi G, Yokosuka T, Saito T, Dustin ML (2006) T cell receptor proximal signals are sustained in peripheral microclusters and terminated in the central supramolecular activation cluster. *Immunity* 25:117–127.
10. Kaizuka Y, Douglass AD, Varma R, Dustin ML, Vale RD (2007) Mechanisms for segregating T cell receptor and adhesion molecules during immunological synapse formation in Jurkat T cells. *Proc Natl Acad Sci USA* 104:20296–20301.
11. Evans R, et al. (2009) Integrins in immunity. *J Cell Sci* 122:215–225.
12. Ilani T, Khanna C, Zhou M, Veenstra TD, Bretscher A (2007) Immune synapse formation requires ZAP-70 recruitment by ezrin and CD43 removal by moesin. *J Cell Biol* 179:733–746.
13. DeMond AL, Mossman KD, Starr T, Dustin ML, Groves JT (2008) T cell receptor microcluster transport through molecular mazes reveals mechanism of translocation. *Biophys J* 94:3286–3292.
14. Campi G, Varma R, Dustin ML (2005) Actin and agonist MHC-peptide complex-dependent T cell receptor microclusters as scaffolds for signaling. *J Exp Med* 202:1031–1036.
15. Kim M, Carman CV, Springer TA (2003) Bidirectional transmembrane signaling by cytoplasmic domain separation in integrins. *Science* 301:1720–1725.
16. Dustin ML, Bromley SK, Davis MM, Zhu C (2001) Identification of self through two-dimensional chemistry and synapses. *Annu Rev Cell Dev Biol* 17:133–157.
17. Nye JA, Groves JT (2008) Kinetic control of histidine-tagged protein surface density on supported lipid bilayers. *Langmuir* 24:4145–4149.
18. Pont S, et al. (1986) Identification of 5-topographic domains of the mouse LFA-1 molecule - subunit assignment and functional involvement in lymphoid-cell interactions. *J Immunol* 136:3750–3759.
19. Demond AL, Groves JT (2007) Interrogating the T cell synapse with patterned surfaces and photoactivated proteins. *Curr Opin Immunol* 19:722–727.
20. Groves JT, Ulman N, Cremer P, Boxer SG (1998) Substrate-membrane interactions: mechanisms for imposing patterns on a fluid bilayer membrane. *Langmuir* 12:3347–3350.
21. Groves JT, Ulman N, Boxer SG (1997) Micropatterning fluid lipid bilayers on solid supports. *Science* 275:651–653.
22. Groves JT, Boxer SG (2002) Micropattern formation in supported lipid membranes. *Acct Chem Res* 35:149–157.
23. Galush WJ, Nye JA, Groves JT (2008) Quantitative fluorescence microscopy using supported lipid bilayer standards. *Biophys J* 95:2512–2519.
24. Brown CM, et al. (2006) Probing the integrin-actin linkage using high-resolution protein velocity mapping. *J Cell Sci* 119:5204–5214.
25. Hu K, Ji L, Applegate KT, Danuser G, Waterman-Storer CM (2007) Differential transmission of actin motion within focal adhesions. *Science* 315:111–115.
26. Groves JT, Boxer SG, McConnell HM (1997) Electric field-induced reorganization of two-component supported bilayer membranes. *Proc Natl Acad Sci USA* 94:13390–13395.
27. Groves JT, Boxer SG, McConnell HM (1998) Electric field-induced critical demixing in lipid bilayer membranes. *Proc Natl Acad Sci USA* 95:935–938.
28. Yokosuka T, et al. (2008) Spatiotemporal regulation of T cell costimulation by TCR-CD28 microclusters and protein kinase C $\theta$ translocation. *Immunity* 29:589–601.
29. Choudhuri K, Wiseman D, Brown MH, Gould K, van der Merwe PA (2005) T-cell receptor triggering is critically dependent on the dimensions of its peptide-MHC ligand. *Nature* 436:578–572.
30. Qi SY, Groves JT, Chakraborty A (2001) Synaptic pattern formation during cellular recognition. *Proc Natl Acad Sci USA* 98:6548–6553.
31. Weikl TR, Groves JT, Lipowsky R (2002) Pattern formation during adhesion of multicomponent membranes. *Europhys Lett* 59:916–922.
32. Partharasathy R, Groves JT (2004) Protein patterns at lipid bilayer junctions. *Proc Natl Acad Sci USA* 1001:12798–12803.
33. Rasband WS (2009) ImageJ, Image Processing and Analysis in Java (National Institutes of Health, Bethesda, MD). Available at http://rsb.info.nih.gov/ij/.